Measurement of the $D^0 \to K^-\pi^+e^+e^-$ branching fraction and search for $D^0 \to \pi^+\pi^-e^+e^-$ and $D^0 \to K^+K^-e^+e^-$ decays at Belle

I. Adachi, L. Aggarwal, H. Ahmed, Y. Ahn, H. Aihara, N. Akopov, S. Alghamdi, M. Alhakami, A. Aloisio, N. Althubiti, K. Amos, M. Angelsmark, N. Anh Ky, C. Antonioli, D. M. Asner, H. Atmacan, T. Aushev, V. Aushev, M. Aversano, R. Ayad, V. Babu, H. Bae, N. K. Baghel, S. Bahinipati, P. Bambade, Sw. Banerjee, S. Bansal, M. Barrett, M. Bartl, J. Baudot, A. Baur, A. Beaubien, F. Becherer, J. Becker, J. V. Bennett, F. U. Bernlochner, V. Bertacchi, M. Bertemes, E. Bertholet, M. Bessner, S. Bettarini, V. Bhardwaj, B. Bhuyan, F. Bianchi, L. Bierwirth, T. Bilka, D. Biswas, A. Bobrov, D. Bodrov, A. Bolz, A. Bondar, J. Borah, A. Boschetti, A. Bozek, M. Bračko, P. Branchini, N. Brenny, R. A. Briere, T. E. Browder, A. Budano, S. Bussino, Q. Campagna, M. Campajola, L. Cao, G. Casarosa, C. Cecchi, J. Cerasoli, M.-C. Chang, P. Chang, R. Cheaib, P. Cheema, C. Chen, L. Chen, B. G. Cheon, K. Chilikin, J. Chin, K. Chirapatpimol, H.-E. Cho, K. Cho, S.-J. Cho, S.-K. Choi, S. Choudhury, J. Cochran, I. Consigny, L. Corona, J. X. Cui, E. De La Cruz-Burelo, S. A. De La Motte, G. de Marino, G. De Nardo, G. De Pietro, R. de Sangro, M. Destefanis, S. Dey, R. Dhamija, A. Di Canto, F. Di Capua, J. Dingfelder, Z. Doležal, I. Domínguez Jiménez, T. V. Dong, X. Dong, K. Dort, D. Dossett, S. Dubey, K. Dugic, G. Dujany, P. Ecker, M. Eliachevitch, D. Epifanov, R. Farkas, P. Feichtinger, T. Ferber, T. Fillinger, C. Finck, G. Finocchiaro, A. Fodor, F. Forti, A. Frey, B. G. Fulsom, A. Gabrielli, E. Ganiev, M. Garcia-Hernandez, R. Garg, G. Gaudino, V. Gaur, V. Gautam, A. Gellrich, G. Ghevondyan, D. Ghosh, H. Ghumaryan, G. Giakoustidis, R. Giordano, A. Giri, P. Gironella Gironell, A. Glazov, B. Gobbo, R. Godang, O. Gogota, P. Goldenzweig, E. Graziani, D. Greenwald, Z. Gruberová, T. Gu, Y. Guan, K. Gudkova, I. Haide, S. Halder, Y. Han, T. Hara, C. Harris, K. Hayasaka, H. Hayashii, S. Hazra, M. T. Hedges, A. Heidelbach, I. Heredia de la Cruz, M. Hernández Villanueva, T. Higuchi, M. Hoek, M. Hohmann, R. Hoppe, P. Horak, C.-L. Hsu, A. Huang, T. Humair, T. Iijima, K. Inami, G. Inguglia, N. Ipsita, A. Ishikawa, R. Itoh, M. Iwasaki, P. Jackson, D. Jacobi, W. W. Jacobs, E.-J. Jang, Q. P. Ji, S. Jia, Y. Jin, A. Johnson, K. K. Joo, H. Junkerkalefeld, A. B. Kaliyar, J. Kandra, K. H. Kang, S. Kang, G. Karyan, T. Kawasaki, F. Keil, C. Ketter, C. Kiesling, C.-H. Kim, D. Y. Kim, J.-Y. Kim, K.-H. Kim, Y. J. Kim, Y.-K. Kim, H. Kindo, K. Kinoshita, P. Kodyš, T. Koga, S. Kohani, K. Kojima, A. Korobov, S. Korpar, E. Kovalenko, R. Kowalewski, P. Križan, P. Krokovny, T. Kuhr, Y. Kulii, D. Kumar, J. Kumar, M. Kumar, R. Kumar, K. Kumara, T. Kunigo, A. Kuzmin, Y.-J. Kwon, S. Lacaprara, Y.-T. Lai, K. Lalwani, T. Lam, L. Lanceri, J. S. Lange, T. S. Lau, M. Laurenza, K. Lautenbach, R. Leboucher, F. R. Le Diberder, M. J. Lee, C. Lemettais, P. Leo, D. Levit, P. M. Lewis, C. Li, H.-J. Li, L. K. Li, Q. M. Li, S. X. Li, W. Z. Li, Y. Li, Y. B. Li, Y. P. Liao, J. Libby, J. Lin, S. Lin, Z. Liptak, M. H. Liu, Q. Y. Liu, Y. Liu, Z. Q. Liu, D. Liventsev, S. Longo, A. Lozar, T. Lueck, C. Lyu, Y. Ma, C. Madaan, M. Maggiora, S. P. Maharana, R. Maiti, S. Maity, G. Mancinelli, R. Manfredi, E. Manoni, M. Mantovano, D. Marcantonio, S. Marcello, C. Marinas, C. Martellini, A. Martens, A. Martini, T. Martinov, L. Massaccesi, M. Masuda, T. Matsuda, D. Matvienko, S. K. Maurya, M. Maushart, J. A. McKenna, R. Mehta, F. Meier, D. Meleshko, M. Merola, C. Miller, M. Mirra, S. Mitra, K. Miyabayashi, H. Miyake, R. Mizuk, G. B. Mohanty, S. Mondal, S. Moneta, H.-G. Moser, M. Mrvar, R. Mussa, I. Nakamura, M. Nakao, Y. Nakazawa, M. Naruki, Z. Natkaniec, A. Natochii, M. Nayak, G. Nazaryan, M. Neu, C. Niebuhr, M. Niiyama, S. Nishida, S. Ogawa, Y. Onishchuk, H. Ono, Y. Onuki, F. Otani, E. R. Oxford, P. Pakhlov, G. Pakhlova, E. Paoloni, S. Pardi, K. Parham, H. Park, J. Park, K. Park, S.-H. Park, B. Paschen, A. Passeri, S. Patra, S. Paul, T. K. Pedlar, I. Peruzzi, R. Peschke, R. Pestotnik, M. Piccolo, L. E. Piilonen, G. Pinna Angioni, P. L. M. Podesta-Lerma, T. Podobnik, S. Pokharel, A. Prakash, C. Praz, S. Prell, E. Prencipe, M. T. Prim, S. Privalov, I. Prudiiev, H. Purwar, P. Rados, G. Raeuber, S. Raiz, N. Rauls, K. Ravindran, J. U. Rehman, M. Reif, S. Reiter, M. Remnev, L. Reuter, D. Ricalde Herrmann, I. Ripp-Baudot, G. Rizzo, S. H. Robertson, M. Roehrken, J. M. Roney, A. Rostomyan, N. Rout, L. Salutari, D. A. Sanders, S. Sandilya, L. Santelj, Y. Sato, V. Savinov, B. Scavino, C. Schmitt, J. Schmitz, S. Schneider, G. Schnell, M. Schnepf, C. Schwanda, A. J. Schwartz, Y. Seino, A. Selce, K. Senyo, J. Serrano, M. E. Sevior, C. Sfienti, W. Shan,

C. Sharma, G. Sharma, C. P. Shen, X. D. Shi, T. Shillington, T. Shimasaki, J.-G. Shiu, D. Shtol, B. Shwartz, A. Sibidanov, F. Simon, J. B. Singh, J. Skorupa, M. Sobotzik, A. Soffer, A. Sokolov, E. Solovieva, W. Song, S. Spataro, B. Spruck, M. Starič, P. Stavroulakis, S. Stefkova, R. Stroili, J. Strube, Y. Sue, M. Sumihama, K. Sumisawa, W. Sutcliffe, N. Suwonjandee, H. Svidras, M. Takahashi, M. Takizawa, U. Tamponi, K. Tanida, F. Tenchini, A. Thaller, O. Tittel, R. Tiwary, E. Torassa, K. Trabelsi, F. F. Trantou, I. Tsaklidis, M. Uchida, I. Ueda, T. Uglov, K. Unger, Y. Unno, K. Uno, S. Uno, P. Urquijo, Y. Ushiroda, S. E. Vahsen, R. van Tonder, M. Veronesi, A. Vinokurova, V. S. Vismaya, L. Vitale, V. Vobbilisetti, R. Volpe, A. Vossen, B. Wach, M. Wakai, S. Wallner, E. Wang, M.-Z. Wang, X. L. Wang, Z. Wang, A. Warburton, M. Watanabe, S. Watanuki, C. Wessel, E. Won, X. P. Xu, B. D. Yabsley, S. Yamada, W. Yan, W. C. Yan, S. B. Yang, J. Yelton, K. Yi, J. H. Yin, K. Yoshihara, J. Yuan, L. Zani, F. Zeng, M. Zeyrek, B. Zhang, V. Zhilich, J. S. Zhou, Q. D. Zhou, L. Zhu, V. I. Zhukova, and R. Žlebčík

(The Belle and Belle II Collaborations)

We present a study of the rare charm meson decays $D^0 \to K^+K^-e^+e^-$, $\pi^+\pi^-e^+e^-$, and $K^-\pi^+e^+e^-$ using a 942 fb^{-1} data set collected by the Belle detector at the KEKB asymmetric-energy e^+e^- collider. We use D^0 candidates identified by the charge of the pion in $D^* \to D^0\pi$ decays and normalize the branching fractions to $D^0 \to K^-\pi^+\pi^-\pi^+$ decays. The branching fraction for decay $D^0 \to K^-\pi^+e^+e^-$ is measured to be $(39.6 \pm 4.5\,(\text{stat}) \pm 2.9\,(\text{syst})) \times 10^{-7}$, with the dielectron mass in the ρ/ω mass region $675 < m_{ee} < 875\,\text{MeV}/c^2$. We also search for $D^0 \to h^-h^{(\prime)+}e^+e^-$ ($h^{(\prime)} = K, \pi$) decays with the dielectron mass near the η and ϕ resonances, and away from these resonances for the $K^+K^-e^+e^-$ and $\pi^+\pi^-e^+e^-$ modes. For these modes, we find no significant signals and set 90% confidence level upper limits on their branching fractions at the $\mathcal{O}(10^{-7})$ level.

Electroweak penguin quark transitions mediated by flavor changing neutral currents (FCNCs) such as $b \to s\,\ell^+\ell^-$, $b \to d\,\ell^+\ell^-$, and $c \to u\,\ell^+\ell^-$ (where $\ell^\pm$ is an electron or muon) are forbidden at tree level in the standard model (SM) [1]. The FCNCs proceed through electroweak box or loop diagrams and are thus highly suppressed, and thus $c \to u\,\ell^+\ell^-$ decays probe beyond the standard model (BSM) physics that could affect the decay rate and other variables. The BSM amplitudes can interfere with the SM amplitudes, altering physics observables from the SM predictions such as total and differential decay rates, and affecting tests of lepton flavor universality (LFU) [2–6].

The decays $c \to u\,\ell^+\ell^-$ are FCNC transitions of a charm quark to an up quark and a lepton pair. Compared to $b \to s\,\ell^+\ell^-$ and $b \to d\,\ell^+\ell^-$ decays, these transitions are further suppressed due to the Glashow–Iliopoulos–Maiani mechanism and the small quark masses relative to the top quark in the loop [7]. The decays $D^0 \to X^0\ell^+\ell^-$, where X^0 is a light-quark system, can have contributions from both short-distance (SD) and long-distance (LD) amplitudes, as shown in Fig. 1. The SD decay amplitudes are suppressed, with branching fractions ($\mathcal{B}$) reaching only the 2×10^{-9} level [8]. However, LD contributions from photon pole or vector meson dominance (VMD) amplitudes, which proceed through the decays $D^0 \to X^0(\gamma^*/V^0) \to X^0\ell^+\ell^-$, where γ^* is an off-shell virtual photon and V^0 is an intermediate vector meson (ρ, ω, ϕ), can reach values of up to 2×10^{-6} [8] for the Cabibbo-favored decay $D^0 \to K^-\pi^+e^+e^-$.

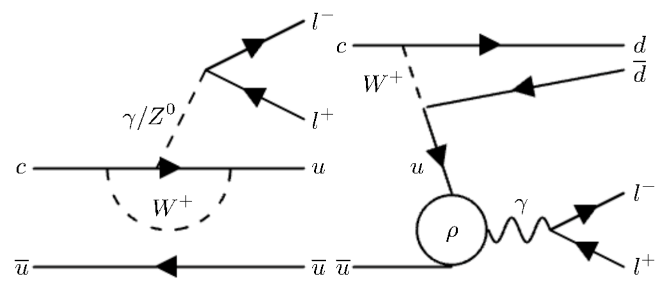

FIG. 1. SD contributions to FCNC D^0 decays through an electroweak penguin diagram (left). LD contributions to $D^0 \to X^0V^0 \to X^0l^+l^-$ decays through the VMD diagram (right).

Several BSM scenarios such as the minimal supersymmetric standard model, models including leptoquarks, little Higgs, Z' models, and models with warped extra dimensions predict significantly enhanced rates for $c \to u\,\ell^+\ell^-$ decays [2–6, 9–11]. Thus, measurements of branching fractions for these decays allow us to probe for BSM physics and to characterize the LD contributions to the decay amplitudes.

The *BABAR* [12–15], BES III [16], CLEO II [17], D0 [18], Fermilab E653 [19], E791 [20], and LHCb [21–25] Collaborations have searched for rare and forbidden $X_c \to h\,(h^{(\prime)})\,\ell^+\ell^{-(\prime)}$ decays in several final states. BES III sets upper limits (UL) at the 90% confidence level (CL) in the range $(11 - 41) \times 10^{-6}$ for $D^0 \to h^-h^{(\prime)+}e^+e^-$ decays [16]. Recently, several four-body decays $D^0 \to hh^{(\prime)}\ell^+\ell^-$ (where $hh^{(\prime)} = KK, \pi\pi, K\pi$) have been observed. BABAR observed the decay $D^0 \to K^-\pi^+e^+e^-$ in the mass range $675 < m_{ee} < 875$ MeV/c^2 at a rate compatible with VMD contributions, and set a branching fraction upper limit on $D^0 \to K^-\pi^+e^+e^-$, excluding e^+e^- resonances with branching fractions above 3.1×10^{-6} at the 90% confidence level [13]. LHCb observed the decay $D^0 \to K^-\pi^+\mu^+\mu^-$ [21], and also observed the decays $D^0 \to \pi^+\pi^-\mu^+\mu^-$ and $D^0 \to K^+K^-\mu^+\mu^-$ [22].

Here we search for the rare charm meson decays $D^0 \to K^+K^-e^+e^-$, $\pi^+\pi^-e^+e^-$, and $K^-\pi^+e^+e^-$ using data collected by the Belle experiment. We analyze the $e^+e^- \to c\bar{c}$ data that has a total integrated luminosity of 942 fb^{-1}. The data was collected at center-of-mass energies ($E_{\rm cm}$) at the $\Upsilon(4S)$ resonances or 60 MeV below, at the $\Upsilon(5S)$ resonance, and in the $10860 < E_{\rm cm} < 11020$ MeV energy scan. The data was recorded from 2000 to 2010 from the collision of 8 GeV electrons with 3.5 GeV positrons at the KEKB collider [26]. The Belle detector, a large-solid-angle magnetic spectrometer, is described in detail elsewhere [27]. The Belle inner detector consists of a four-layer silicon vertex detector, a 50-layer central drift chamber, an array of aerogel threshold Cerenkov counters, a barrel-like arrangement of time-of-flight scintillation counters, and an electromagnetic calorimeter composed of CsI (Tl) crystals, all located inside a superconducting solenoid coil that provides a 1.5 T magnetic field. An iron flux-return yoke placed outside the coil is instrumented with resistive plate chambers to detect K^0_L mesons and muons.

We use Monte Carlo (MC) simulated events to optimize selection criteria, calculate reconstruction efficiencies, and study background sources. We generate the MC event samples using `EvtGen` [28], `PYTHIA` [29], and we use `PHOTOS` [30] and `Geant3` [31] to simulate final state radiation and the detector response, respectively. For each signal channel we generate $hh^{(\prime)}$ and ee resonant and non-resonant signal MC samples. We neglect interference between non-resonant and resonant decays. We use MC samples of $e^+e^- \to q\bar{q}$ (where $q = u, d, s$ or c) and $e^+e^- \to B\overline{B}$ corresponding to six times that of the data to study the background composition.

We require at least five charged tracks in the event. Each track must have a momentum greater than 0.1 GeV/c. We require the distance of the closest approach to the origin to be less than 4.5 cm along the beam direction and less than 0.25 cm transverse to the beam direction to reduce beam-induced backgrounds and background from K^0_S mesons. We perform particle identification (PID) based on information provided by detector subsystems in the form of likelihoods $\mathcal{L}_i$ for species i, where $i = e$, μ, π, K, or p for each track. Kaon candidates must have $\mathcal{R}_K = \mathcal{L}_K/(\mathcal{L}_K + \mathcal{L}_\pi) > 0.1$ for the $K^-\pi^+e^+e^-$ and $K^+K^-e^+e^-$ mode, and pion candidates are required to have $\mathcal{R}_K < 0.4$ for the $\pi^+\pi^-e^+e^-$ mode. These requirements have kaon and pion identification efficiencies of about 97% and 91%, with misidentification rates of about 20% and 10%, respectively. The electron candidates must have $\mathcal{R}_e = \mathcal{L}_e/(\mathcal{L}_e + \mathcal{L}_\mu + \mathcal{L}_K + \mathcal{L}_\pi + \mathcal{L}_p) > 0.8$. To recover electron bremsstrahlung, we add photon(s) having a minimum energy of 20 MeV and an angle within 5 degrees around the direction of the electron track at the IP to the four-momenta of the electron candidate. The electron identification efficiency is about 91%, with a misidentification rate of less than 3%. We use the B2BII software package [32] to convert the Belle data to Belle II data format and analyze the data with the Belle II analysis software framework (`basf2`) [33].

We reconstruct $D^0 \to K^-\pi^+e^+e^-$, $\pi^+\pi^-e^+e^-$, and $K^+K^-e^+e^-$ signal candidates from the selected kaon, pion, and electron candidates. Candidates with D^0 invariant mass $m_{hh^{(\prime)}ee}$ in the range $1.80 < m_{hh^{(\prime)}ee} < 1.93$ GeV/c^2 are combined with a π^+ candidate to form a D^{*+} candidate. The requirement of a D^{*+} tagged D^0 suppresses the background from random track combinations. Candidates must have a D^{*+} momentum in the center-of-mass frame $p^*(D^{*+}) > 2.5$ GeV/c to reduce the combinatorial background from B decays and a mass difference between D^{*+} and D^0 candidates Δm within 0.5 MeV/c^2 of the nominal value [34] to be consistent with the decay $D^{*+} \to D^0\pi^+$. We also apply a vertex fit to the decay chain $D^{*+} \to D^0\pi^+$, $D^0 \to hh^{(\prime)}ee$, with the D^* production vertex constrained to the interaction point. We discard candidates that fail this fit.

The decay $\pi^0/\eta \to e^+e^-\gamma$ can produce a complicated background shape, which is difficult to model. The electron bremsstrahlung recovery can mistakenly include a photon originating from a π^0/η decay so that the reconstructed $m(hh^{(\prime)}ee\gamma)$ will fake the signal. Such decays will also contribute to a background in the $m_{hh^{(\prime)}ee}$ region below the D^0 mass, resulting in a non-linear background shape. To suppress these backgrounds, we apply the selection $m_{ee} > 200$ MeV/c^2. In addition, we do not apply electron bremsstrahlung recovery for candidates with m_{ee} in the η mass region (520, 560 MeV/c^2). The $m_{ee} > 560$ MeV/c^2 is applied to the $K^-\pi^+e^+e^-$ for searching the signal not in the resonant region to suppress the $D^0 \to K^-\pi^+\eta$ [$\to e^+e^-\gamma$] background.

Some candidates include electrons originating from photon conversions. In order to veto these events, we combine the $e^\pm$ from the signal (D^0) candidate with another oppositely charged track from the event to form a candidate e^+e^- pair. We require a converged vertex fit for the photon conversion candidates (e^+e^-) and discard the corresponding D^0 candidate if the angle between the e^+e^- tracks in the lab frame is less than 0.07 radians or the invariant mass of e^+e^- tracks is less than 100 MeV/c^2.

Hadronic D^0 decays in which one or more of the D^0 daughters are misidentified as leptons also contribute to the background. In each event, we reconstruct $D^{*+} \to D^0\pi^+_s$ with $D^0 \to K^-\pi^+\pi^-\pi^+$, $D^0 \to \pi^+\pi^-\pi^+\pi^-$, and $D^0 \to K^+K^-\pi^+\pi^-$ decays in addition to the signal modes $hh^{(\prime)}e^+e^-$. We discard the corresponding signal candidate if any of the reconstructed hadronic D^0 decay candidates have invariant mass and Δm within 3 MeV/c^2 and 0.4 MeV/c^2, respectively, of the corresponding nominal values.

For each signal mode, we optimize the selection criteria for $p^*(D^{*+})$, Δm, PID, photon conversion and hadronic D^0 vetos in the η (520, 560), ρ/ω (675, 875), and ϕ (990, 1035 MeV/c^2) mass regions in order to search for potential ee resonant decays. We also search for $D^0 \to h^- h^{(\prime)+} e^+ e^-$ decays in the m_{ee} spectrum not included in the resonant regions defined above which we refer to as "non-resonant". The m_{ee} regions mentioned above are not individually optimized, with the m_{ee} ranges covering about 80% of the corresponding ee resonance regions. For events with more than one signal candidate, the candidate with Δm closest to the known value is selected. We optimize the cuts by maximizing a figure-of-merit $S/\sqrt{S+B}$ for each m_{ee} region, where S and B are the expected number of signal candidates in data estimated from PDG [34] branching fractions and background yields estimated using background MC samples, respectively. Since the D^0 production rate is not precisely known, we measure the signal branching fractions relative to the normalization decay $D^0 \to K^-\pi^+\pi^-\pi^+$, with similar selections applied such as PID.

We calculate the signal branching fractions and upper limits using the equation

$$\mathcal{B}(hh^{(\prime)}ee) = \frac{N_{hh^{(\prime)}ee}}{N_{K\pi\pi\pi}} \frac{\epsilon_{K\pi\pi\pi}}{\epsilon_{hh^{(\prime)}ee}} \mathcal{B}(K^-\pi^+\pi^-\pi^+), \qquad (1)$$

where N are the yields, and ϵ are the reconstruction efficiencies. We measure the branching fractions or set branching fraction upper limits for various m_{ee} regions in each $hh^{(\prime)}ee$ mode.

We use a one-dimensional unbinned extended maximum likelihood fit to $m_{hh^{(\prime)}ee}$ to extract the signal yield for each decay mode in the η (520, 560), ρ/ω (675, 875), ϕ (990, 1035 MeV/c^2), and remaining m_{ee} regions. The signal probability density function (PDF) is a Gaussian-like function with different resolutions above and below the D^0 mass [35]. We obtain the signal PDF parameters from fits to the signal MC distributions, and we fix these parameters for the signal yield extraction. We model the background using a linear function, where the slope parameter is floated in the fit. We do not examine any signal mode distributions until the analysis procedure is finalized to minimize potential biases on the measured quantities.

We show the signal mode $m_{hh^{(\prime)}ee}$ distributions with projections of the fits superimposed for each m_{ee} region in Fig. 2. For each signal channel, we provide the branching fractions, and the corresponding significance $S = \sqrt{-2\Delta\ln\mathcal{L}}$, where $\Delta\ln\mathcal{L}$ is the difference in the log-likelihood from the maximum value with respect to the value from the background-only hypothesis. We measure the branching fraction of $D^0 \to K^-\pi^+e^+e^-$ in the m_{ee} range $675 < m_{ee} < 875$ MeV/c^2 to be $(39.6 \pm 4.5 \pm 2.9) \times 10^{-7}$, where the first uncertainty is statistical and the second is systematic with a significance of 11.8σ. We set 90% CL upper limits using the CL$_s$ method [36] for the channels with no significant signal; these results are in

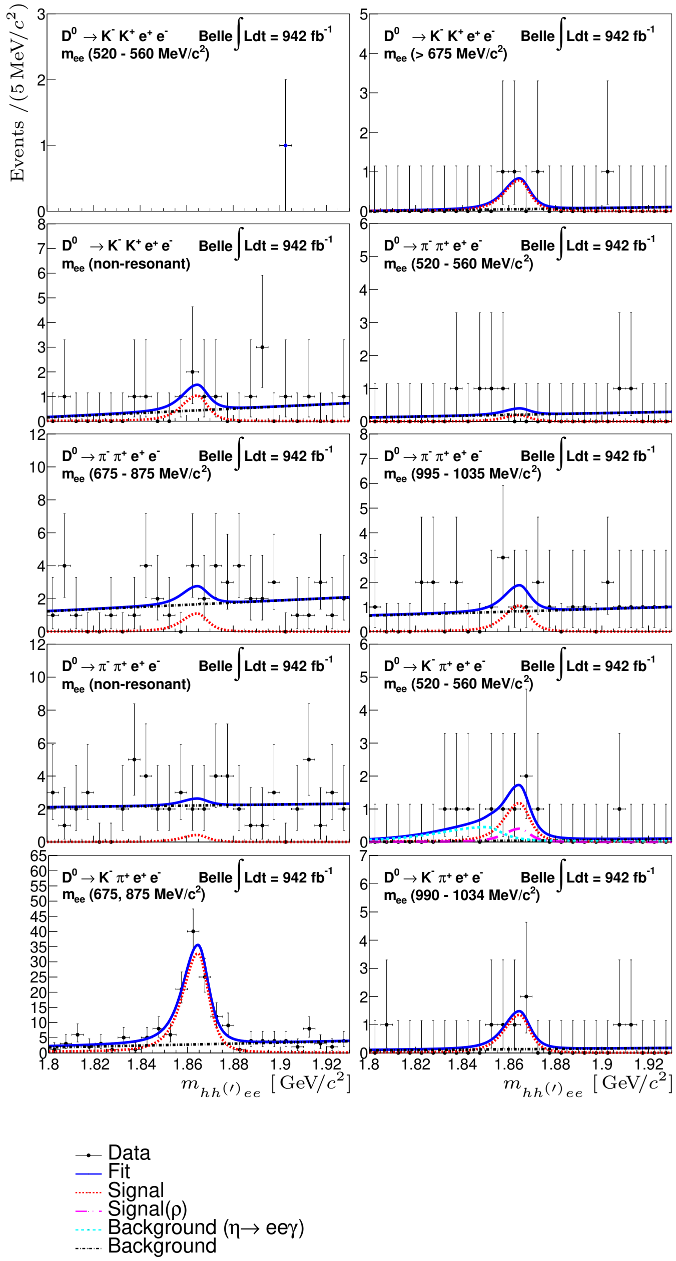

FIG. 2. $D^0 \to hh^{(\prime)}ee$ decays $m_{hh^{(\prime)}ee}$ distributions for m_{ee} in the η, ρ/ω and ϕ mass regions. The $\eta \to e^+e^-\gamma$ decay background is shown for $D^0 \to K^-\pi^+e^+e^-$ with m_{ee} in the η mass region (cyan dashed curve). These background PDF parameters are obtained from $D^0 \to K^-\pi^+\eta$ [$\to e^+e^-\gamma$] MC simulation in which the γ is not reconstructed. The $K^+K^-e^+e^-$ mode with m_{ee} in the η mass region is not fitted since only one event is observed.

the range from $(2.3 - 8.1) \times 10^{-7}$. The extracted signal yields, significances, efficiencies, and branching fractions, or branching fraction upper limits for each m_{ee} region are given in Table I. In the supplemental material, we show the projection of the fit on the $D^0 \to h^- h^{(\prime)+} e^+ e^-$

TABLE I. $D^0 \to h^- h^{(\prime)+} e^+ e^-$ yields, efficiencies, branching fractions, significances, and branching fraction upper limits @ 90% CL of each m_{ee} region. A fitted yield and a branching fraction are not reported for the $K^+K^-e^+e^-$ mode with m_{ee} in the m_η region since only one event is observed, and the significance is determined from the CL_s distribution. The first uncertainty is statistical and the second is systematic.

Decay mode	m_{ee} region (MeV/c^2)	Yield	Efficiency (%)	$\mathcal{B}$ ($\times 10^{-7}$)	Significance	UL ($\times 10^{-7}$)
$K^+K^-e^+e^-$						
η	520-560	-	3.33 ± 0.04	-	0.0σ	2.3
ρ^0/ω	> 675	2.6 ± 1.8	5.68 ± 0.06	1.2 ± 0.9 ± 0.1	2.0σ	3.0
non-resonant	> 200 [a]	3.5 ± 3.3	2.97 ± 0.04	3.1 ± 3.0 ± 0.4	1.5σ	7.7
$\pi^+\pi^-e^+e^-$						
η	520-560	0.6 ± 2.3	4.61 ± 0.05	0.4 ± 1.4 ± 0.2	0.3σ	3.2
ρ^0/ω	675-875	3.7 ± 4.1	4.99 ± 0.05	2.0 ± 2.2 ± 0.8	0.9σ	6.1
ϕ	995-1035	3.6 ± 3.2	8.40 ± 0.06	1.1 ± 1.1 ± 0.2	1.1σ	3.1
non-resonant	> 200	1.4 ± 4.2	3.29 ± 0.04	1.2 ± 3.4 ± 1.1	0.3σ	8.1
$K^-\pi^+e^+e^-$						
η	520-560	4.0 ± 2.7	4.91 ± 0.04	2.2 ± 1.5 ± 0.5	1.6σ	5.6
ρ^0/ω	675-875	110 ± 13	7.53 ± 0.06	39.6 ± 4.5 ± 2.9	11.8σ	-
ϕ	990-1034	4.6 ± 2.4	8.75 ± 0.06	1.4 ± 0.8 ± 0.3	2.5σ	2.9

[a] Excluding resonance regions, which are the same for all three modes.

distribution as a function of m_{ee}^2 with the background subtracted using the *sPlot* technique [37].

Systematic uncertainties can be divided into multiplicative and additive categories. The additive systematic uncertainties affect the determination of the signal and normalization mode yields and the corresponding significance. Multiplicative systematic uncertainties include PID and tracking efficiencies. The systematic uncertainty of tracking efficiency is 0.35% for each track, obtained from a study of a $D^{*+} \to D^0(\pi^+\pi^-K_S^0)\pi^+$ data control sample. The systematic uncertainty due to K identification is 1.0%, determined from a study of a $D^{*+} \to D^0(K^-\pi^+)\pi^+$ control sample. The electron identification efficiency uncertainty is determined from $e^+e^- \to e^+e^-e^+e^-$ processes and found to be 2.0% for each track. The PID efficiency corrections are applied for the normalization mode and for each signal channel, and the particle identification systematics are about 5%, which depend on the decay channel. We do not include a systematic uncertainty for the PID fake rates as the D^0 candidate invariant mass of misidentified $h^-h^{(\prime)+}e^+e^-$ decays do not peak near the D^0 mass after final selections according to MC simulations of hadronic D^0 decays. To account for the potential non-resonant decay contribution in the m_{ee} resonance regions, the signal efficiency differences obtained using the signal MC between non-resonant and resonant decays are included in the systematic uncertainty.

The uncertainty in yield extraction contributes to the additive systematic uncertainty, which affects the significance of the branching fraction. We obtain the PDF-related uncertainties by varying the PDF shapes and parameters for both signal and background. As alternative PDFs, we use two double-sided Crystal Ball functions [38] with a shared mean for the signal and a second-order Chebyshev polynomial for the background PDF functions to determine the signal yield systematics from the PDF shapes. In addition, the yield differences between the signal PDF parameters, fixed and floated, are incorporated into the systematic uncertainty. The additive systematic uncertainty for the background originating from the signal channel $D^0 \to h^-h^{(\prime)+}e^+e^-$ with ee from ρ resonant decay is negligible for other ee resonance regions. To incorporate the systematic uncertainties into the upper limits, the likelihood function is convolved with two Gaussian functions whose widths are the total multiplicative and additive systematic uncertainties and a third Gaussian with a width that is the sum in quadrature of the additive systematic uncertainties from the normalization mode.

In summary, we have measured the branching fraction of $D^0 \to K^-\pi^+e^+e^-$ in the m_{ee} range $675 < m_{ee} < 875$ MeV/c^2 to be

$$(39.6 \pm 4.5 \pm 2.9) \times 10^{-7}$$

with a significance of 11.8σ using 942 fb^{-1} of Belle data. The measured branching fraction is consistent with and more precise than the *BABAR* measurement [13]. For the other ee resonant and non-resonant regions, we do not observe any significant signal and set 90% CL upper limits on the branching fractions. These limits range from 2.3×10^{-7} to 8.1×10^{-7}. Our $D^0 \to K^-\pi^+e^+e^-$ limits are more restrictive than the *BABAR* [14] and BES III [16] limits.

Note added:

While this manuscript was being finalized, LHCb published new results on $D^0 \to \pi^+\pi^-e^+e^-$ and $D^0 \to K^+K^-e^+e^-$ decays. They observe the former in two m_{ee} mass regions and set upper limits on the latter that are 1.4–7.7 times more stringent than ours [25].

ACKNOWLEDGEMENT

This work, based on data collected using the Belle II detector, which was built and commissioned prior to March 2019, and data collected using the Belle detector, which was operated until June 2010, was supported by Higher Education and Science Committee of the Republic of Armenia Grant No. 23LCG-1C011; Australian Research Council and Research Grants No. DP200101792, No. DP210101900, No. DP210102831, No. DE220100462, No. LE210100098, and No. LE230100085; Austrian Federal Ministry of Education, Science and Research, Austrian Science Fund (FWF) Grants DOI: 10.55776/P34529, DOI: 10.55776/J4731, DOI: 10.55776/J4625, DOI: 10.55776/M3153, and DOI: 10.55776/PAT1836324, and Horizon 2020 ERC Starting Grant No. 947006 "InterLeptons"; Natural Sciences and Engineering Research Council of Canada, Compute Canada and CANARIE; National Key R&D Program of China under Contract No. 2024YFA1610503, and No. 2024YFA1610504 National Natural Science Foundation of China and Research Grants No. 11575017, No. 11761141009, No. 11705209, No. 11975076, No. 12135005, No. 12150004, No. 12161141008, No. 12475093, and No. 12175041, and Shandong Provincial Natural Science Foundation Project ZR2022JQ02; the Czech Science Foundation Grant No. 22-18469S, Regional funds of EU/MEYS: OPJAK FORTE CZ.02.01.01/00/22_008/0004632 and Charles University Grant Agency project No. 246122; European Research Council, Seventh Framework PIEF-GA-2013-622527, Horizon 2020 ERC-Advanced Grants No. 267104 and No. 884719, Horizon 2020 ERC-Consolidator Grant No. 819127, Horizon 2020 Marie Sklodowska-Curie Grant Agreement No. 700525 "NIOBE" and No. 101026516, and Horizon 2020 Marie Sklodowska-Curie RISE project JENNIFER2 Grant Agreement No. 822070 (European grants); L'Institut National de Physique Nucléaire et de Physique des Particules (IN2P3) du CNRS and L'Agence Nationale de la Recherche (ANR) under Grant No. ANR-21-CE31-0009 (France); BMFTR, DFG, HGF, MPG, and AvH Foundation (Germany); Department of Atomic Energy under Project Identification No. RTI 4002, Department of Science and Technology, and UPES SEED funding programs No. UPES/R&D-SEED-INFRA/17052023/01 and No. UPES/R&D-SOE/20062022/06 (India); Israel Science Foundation Grant No. 2476/17, U.S.-Israel Binational Science Foundation Grant No. 2016113, and Israel Ministry of Science Grant No. 3-16543; Istituto Nazionale di Fisica Nucleare and the Research Grants BELLE2, and the ICSC – Centro Nazionale di Ricerca in High Performance Computing, Big Data and Quantum Computing, funded by European Union – NextGenerationEU; Japan Society for the Promotion of Science, Grant-in-Aid for Scientific Research Grants No. 16H03968, No. 16H03993, No. 16H06492, No. 16K05323, No. 17H01133, No. 17H05405, No. 18K03621, No. 18H03710, No. 18H05226, No. 19H00682, No. 20H05850, No. 20H05858, No. 22H00144, No. 22K14056, No. 22K21347, No. 23H05433, No. 26220706, and No. 26400255, and the Ministry of Education, Culture, Sports, Science, and Technology (MEXT) of Japan; National Research Foundation (NRF) of Korea Grants No. 2021R1-F1A-1064008, No. 2022R1-A2C-1003993, No. 2022R1-A2C-1092335, No. RS-2016-NR017151, No. RS-2018-NR031074, No. RS-2021-NR060129, No. RS-2023-00208693, No. RS-2024-00354342 and No. RS-2025-02219521, Radiation Science Research Institute, Foreign Large-Size Research Facility Application Supporting project, the Global Science Experimental Data Hub Center, the Korea Institute of Science and Technology Information (K25L2M2C3) and KREONET/GLORIAD; Universiti Malaya RU grant, Akademi Sains Malaysia, and Ministry of Education Malaysia; Frontiers of Science Program Contracts No. FOINS-296, No. CB-221329, No. CB-236394, No. CB-254409, and No. CB-180023, and SEP-CINVESTAV Research Grant No. 237 (Mexico); the Polish Ministry of Science and Higher Education and the National Science Center; the Ministry of Science and Higher Education of the Russian Federation and the HSE University Basic Research Program, Moscow; University of Tabuk Research Grants No. S-0256-1438 and No. S-0280-1439 (Saudi Arabia), and Researchers Supporting Project number (RSPD2025R873), King Saud University, Riyadh, Saudi Arabia; Slovenian Research Agency and Research Grants No. J1-50010 and No. P1-0135; Ikerbasque, Basque Foundation for Science, State Agency for Research of the Spanish Ministry of Science and Innovation through Grant No. PID2022-136510NB-C33, Spain, Agencia Estatal de Investigacion, Spain Grant No. RYC2020-029875-I and Generalitat Valenciana, Spain Grant No. CIDEGENT/2018/020; the Swiss National Science Foundation; The Knut and Alice Wallenberg Foundation (Sweden), Contracts No. 2021.0174 and No. 2021.0299; National Science and Technology Council, and Ministry of Education (Taiwan); Thailand Center of Excellence in Physics; TUBITAK ULAKBIM (Turkey); National Research Foundation of Ukraine, Project No. 2020.02/0257, and Ministry of Education and Science of Ukraine; the U.S. National Science Foundation and Research Grants No. PHY-1913789 and No. PHY-2111604, and the U.S. Department of Energy and Research Awards No. DE-AC06-76RLO1830, No. DE-SC0007983, No. DE-SC0009824, No. DE-SC0009973, No. DE-SC0010007, No. DE-SC0010073, No. DE-SC0010118, No. DE-SC0010504, No. DE-SC0011784, No. DE-SC0012704, No. DE-SC0019230, No. DE-SC0021274, No. DE-SC0021616, No. DE-SC0022350, No. DE-SC0023470; and the Vietnam Academy of Science and Technology (VAST) under Grants No. NVCC.05.12/22-23 and No. DL0000.02/24-25.

These acknowledgements are not to be interpreted as an endorsement of any statement made by any of our institutes, funding agencies, governments, or their representatives.

We thank the SuperKEKB team for delivering high-luminosity collisions; the KEK cryogenics group for the efficient operation of the detector solenoid magnet and IBBelle on site; the KEK Computer Research Center for on-site computing support; the NII for SINET6 network support; and the raw-data centers hosted by BNL, DESY, GridKa, IN2P3, INFN, PNNL/EMSL, and the University of Victoria.

---

[1] The inclusion of the charge-conjugate decay mode is implemented throughout the letter unless otherwise stated.
[2] S. de Boer and G. Hiller, Phys. Rev. D **98**, 035041 (2018).
[3] A. Paul, I. I. Bigi, and S. Recksiegel, Phys. Rev. D **83**, 114006 (2011).
[4] S. Fajfer, N. Košnik, and S. Prelovšek, Phys. Rev. D **76**, 074010 (2007).
[5] L. Cappiello, O. Catà, and G. D'Ambrosio, J. High Energ. Phys. **2013** (4), 135.
[6] R. Bause, M. Golz, G. Hiller, and A. Tayduganov, Eur. Phys. J. C **80**, 65 (2020).
[7] G. Burdman, E. Golowich, J. Hewett, and S. Pakvasa, Phys. Rev. D **66**, 014009 (2002).
[8] S. Fajfer, A. Prapotnik, S. Prelovšek, P. Singer, and J. Zupan, Nucl. Phys. Proc. Suppl. **115**, 93 (2003).
[9] S. Fajfer, E. Solomonidi, and L. Vale Silva, Phys. Rev. D **109**, 036027 (2024).
[10] R. Bause, M. Golz, G. Hiller, and A. Tayduganov, Eur. Phys. J. 10.1140/epjc/s10052-020-7621-7 (2019).
[11] S. de Boer and G. Hiller, Phys. Rev. D **93**, 074001 (2016).
[12] J. P. Lees *et al.* (*BABAR* Collaboration), Phys. Rev. D **84**, 072006 (2011).
[13] J. P. Lees *et al.* (*BABAR* Collaboration), Phys. Rev. Lett. **122**, 081802 (2019).
[14] J. P. Lees *et al.* (*BABAR* Collaboration), Phys. Rev. Lett. **124**, 071802 (2020).
[15] J. P. Lees *et al.* (*BABAR* Collaboration), Phys. Rev. D **101**, 112003 (2020).
[16] M. Ablikim *et al.* (BESIII Collaboration), Phys. Rev. D **97**, 072015 (2018).
[17] A. Freyberger *et al.* (CLEO Collaboration), Phys. Rev. Lett. **76**, 3065 (1996), [Erratum: Phys. Rev. Lett. **77**, 2147(1996)].
[18] V. M. Abazov *et al.* (D0 Collaboration), Phys. Rev. Lett. **100**, 101801 (2008).
[19] K. Kodama *et al.* (E653 Collaboration), Phys. Lett. B **345**, 85 (1995).
[20] E. M. Aitala *et al.* (E791 Collaboration), Phys. Rev. Lett. **86**, 3969 (2001).
[21] R. Aaij *et al.* (LHCb Collaboration), Phys. Lett. B **757**, 558 (2016).
[22] R. Aaij *et al.* (LHCb Collaboration), Phys. Rev. Lett. **119**, 181805 (2017).
[23] R. Aaij *et al.* (LHCb Collaboration), Phys. Rev. D **97**, 091101 (2018).
[24] R. Aaij *et al.* (LHCb Collaboration), J. High Energ. Phys **2021**, 44 (2021).
[25] R. Aaij *et al.* (LHCb Collaboration), Phys. Rev. D **111**, L091101 (2025).
[26] A. Abashian *et al.* (Belle Collaboration), Nucl. Instrum. Meth. A **499**, 191 (2003), also see Section 2 in J. Brodzicka *et al.*, Prog. Theor. Exp. Phys. **2012**, 04D001 (2012).
[27] S. Kurokawa and E. Kikutani, Nucl. Instrum. Meth. A **499**, 1 (2003).
[28] D. J. Lange, Nucl. Instrum. Meth. A **462**, 152 (2001).
[29] T. Sjöstrand, L. Lönnblad, S. Mrenna, and P. Skands, (2003), arXiv:hep-ph/0308153 [hep-ph].
[30] P. Golonka and Z. Was, Eur. Phys. J. C **45**, 97 (2006).
[31] R. Brun *et al.*, CERN Report No. DD/EE/84-1 (1987).
[32] M. Gelb *et al.*, Comput. Softw. Big Sci. **2**, 9 (2018).
[33] T. Kuhr, C. Pulvermacher, M. Ritter, T. Hauth, and N. Braun (Belle-II Framework Software Group), Comput. Softw. Big Sci. **3**, 1 (2019).
[34] R. L. Workman *et al.* (Particle Data Group), PTEP **2022**, 083C01 (2022).
[35] The normalization mode signal PDF is a sum of the signal PDF used for the signal channels and a Gaussian with a shared mean for the D^0 mass.
[36] A. L. Read, J. Phys. G: Nucl. Part. Phys **28**, 2693 (2002).
[37] M. Pivk and F. Le Diberder, Nucl. Instrum. Methods Phys. Res., Sect A **555**, 356 (2005).
[38] T. Skwarnicki, DESY-F31-86-02 (1986).

Supplemental material to $D^0 \to h^- h^{(\prime)+} e^+ e^-$

$D^0 \to h^- h^{(\prime)+} e^+ e^-$ MODES dN/dm_{ee}^2 VS m_{ee}^2 DISTRIBUTIONS

Figure 1 (below) shows the $D^0 \to h^- h^{(\prime)+} e^+ e^-$ modes dN/dm_{ee}^2 vs m_{ee}^2 distributions with background subtracted using the *s𝒫lot* technique.

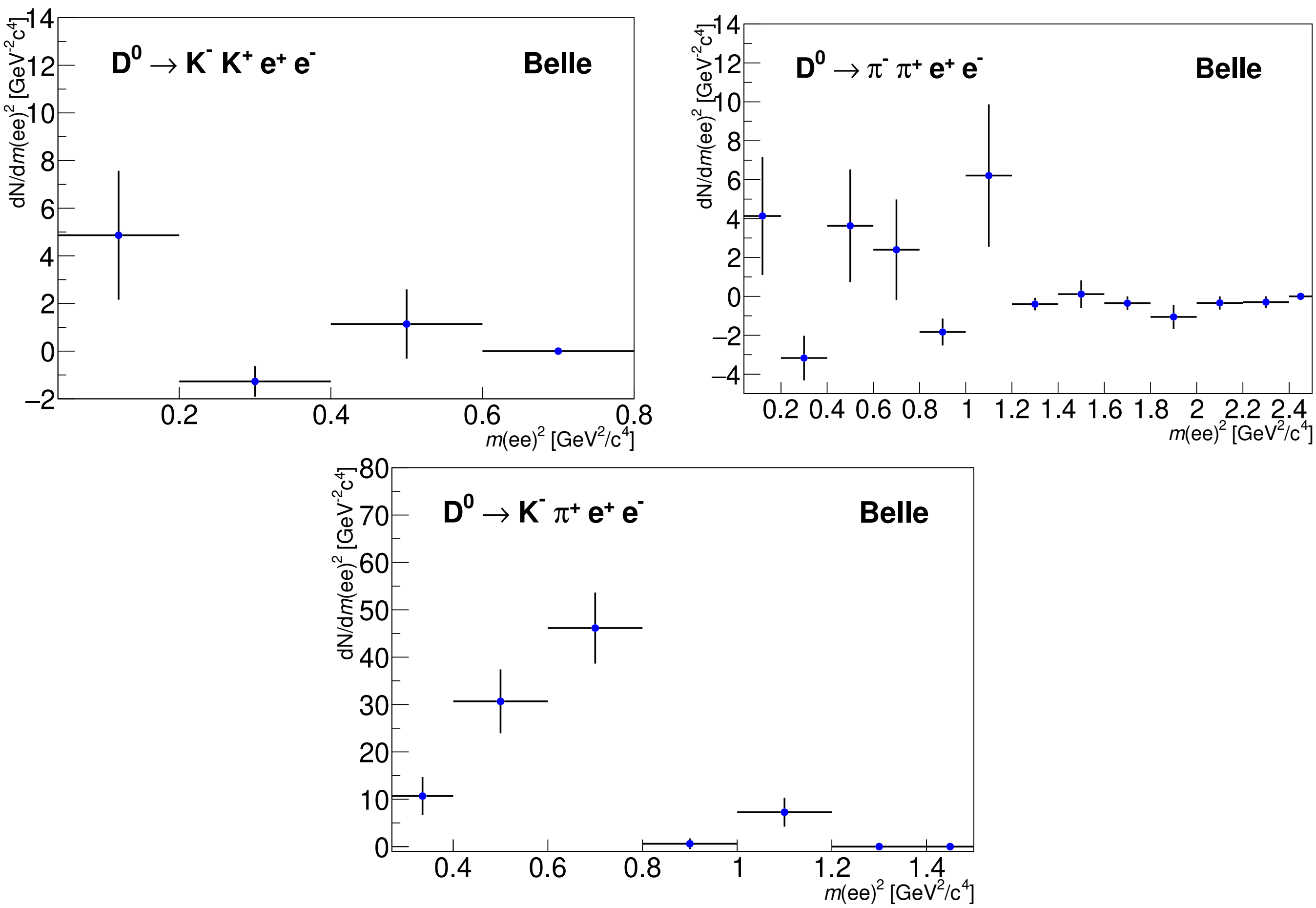

FIG. 1. dN/dm_{ee}^2 vs m_{ee}^2 distributions for $D^0 \to h^- h^{(\prime)+} e^+ e^-$ candidates. The background has been subtracted using the *s𝒫lot* technique. A significant $D^0 \to K^- \pi^+ e^+ e^-$ signal with m_{ee} in ρ/ω mass region is visible in the (0.4, 0.8 GeV$^2/c^4$) m_{ee}^2 bins. The negative bins are due to low statistics after final selections. In the analysis, the selections are optimized separately in each resonance region and in the combined non-resonant regions. For these plots, the $p^*(D^{*+})$, Δm, and PID selections for the non-resonant region are applied to all m_{ee} regions.